eSCAN: Scan Regulatory Regions for Aggregate Association Testing using Whole Genome Sequencing Data

Yingxi Yang,[1*] Yuchen Yang,[2,3,4*] Le Huang,[2] Jai G. Broome[5,6], Adolfo Correa,[7] Alexander Reiner,[8,9] NHLBI Trans-Omics for Precision Medicine (TOPMed) Consortium, Laura M. Raffield[2*], Yun Li[2,10,11*†]

[1]Department of Statistics, Sun Yat-Sen University, Guangzhou, Guangdong, 510275, China

[2] Department of Genetics, University of North Carolina at Chapel Hill, Chapel Hill, NC, 27599, USA

[3] Department of Pathology and Laboratory Medicine, University of North Carolina at Chapel Hill, Chapel Hill, NC, 27599, USA

[4] McAllister Heart Institute, University of North Carolina at Chapel Hill, Chapel Hill, NC, 27599, USA

[5] Department of Biostatistics, University of Washington, Seattle, WA 98195, USA

[6] Department of Medicine, Division of Medical Genetics, University of Washington, Seattle, WA 98195, USA

[7] Department of Medicine and Population Health Science, University of Mississippi Medical Center, Jackson, MS, 39216, USA

[8] Department of Epidemiology, University of Washington, Seattle, WA, 98195, USA

[9] Fred Hutchinson Cancer Research Center, University of Washington, Seattle, WA, 98195, USA

[10] Department of Biostatistics, University of North Carolina at Chapel Hill, Chapel Hill, NC, 27599, USA

[11] Department of Computer Science, University of North Carolina at Chapel Hill, Chapel Hill, NC, 27599, USA

* These authors contributed equally to this work.

† Corresponding author: Yun Li. E-mail: yunli@med.unc.edu

Abstract

With advances in whole genome sequencing (WGS) technology, multiple statistical methods for aggregate association testing have been developed. Many common approaches aggregate variants in a given genomic window of a fixed/varying size and are not reliant on existing knowledge to define appropriate test units, resulting in most identified regions not being clearly linked to genes, limiting biological understanding. Functional information from new technologies (such as Hi-C and its derivatives), which can help link enhancers to the genes they affect, can be leveraged to predefine variant sets for aggregate testing in WGS. Therefore, in this paper we propose the eSCAN (Scan the Enhancers) method for genome-wide assessment of enhancer regions in sequencing studies, combining the advantages of dynamic window selection in SCANG with the advantages of increased incorporation of genomic annotation. eSCAN searches biologically meaningful searching windows, increasing power and aiding biological interpretation, as demonstrated by simulation studies under a wide range of scenarios. We also apply eSCAN for association analysis of blood cell traits using TOPMed WGS data from Women's Health Initiative (WHI) and Jackson Heart Study (JHS). Results from this real data example show that eSCAN is able to capture more

significant signals, and these signals are of shorter length and drive association of larger regions detected by other methods.

Main text

In genome-wide association studies (GWAS), most significantly associated variants are located outside coding regions of genes, making it difficult to interpret the biological function of associated variants. Statistical power to detect rare variant associations in noncoding regions, which is of increasing importance with the advent of large-scale whole genome sequencing (WGS) studies, is also limited with a standard single variant GWAS approach. Aggregate testing is necessary to increase statistical power to detect rare variant associations; linking noncoding variants to their likely effector genes is necessary for interpretation of identified aggregate signals. Many standard methods for aggregate analysis of the noncoding genome are agnostic to regulatory and functional annotation (for example, standard sliding window analysis, where all variants in a given location bin (for example a 5 kb or 10 kb window) are analyzed, followed by analysis of a subsequent partially overlapping window, until each chromosome is assessed in full)[1-3]. SCANG has recently been proposed as an improvement on conventional sliding-window procedures, with the ability to detect the existence and locations of association regions with increased statistical power [4]. SCANG allows sliding-windows to have different sizes within a pre-specified range and then searches all the possible windows across the genome, increasing statistical power. However, since SCANG tests all possible windows, it can "randomly" identify some regions across the genome regardless of their biological functions. Identified regions could often cross multiple enhancer regions with distinct functions, thus impeding the identification of biologically important enhancers and their target genes. This cross-boundary issue may also lead to a higher false positive rate in a fine-mapping sense. The whole region/chromosome in which

the detected regions are located may not be a false positive, but locations of the detected regions will not match the true association regions. Moreover, SCANG applies SKAT to all candidate windows, but computing p-values in SKAT requires eigen decomposition[5]. This analysis method is therefore very time-consuming and has high computational costs, which may not be feasible for increasingly large genome-wide studies.

In addition to sliding window approaches, many analyses of WGS data rely on aggregate tests of predefined variant sets, attempting to link the most likely regulatory variants (as defined by tissue specific histone marks, open chromatin data, sequence conservation, etc) to genes prior to association testing, with variants assigned to genes based on either physical proximity or chromatin conformation[1; 3]. There is increasing data available to define these tissue specific regulatory regions, which are known to show enrichment for GWAS identified noncoding variant signals.[6-8] Recent biotechnological advances based on Chromatin Conformation Capture (3C), such as promoter capture Hi-C data, can also better link gene promoters to enhancers based on their physical interactions in 3D space [9]. We here propose an extension of SCANG which combines the advantages of both scanning and fixed variant set methods (see **Fig. 1** for illustration). Our eSCAN (or "scan the enhancers" with "enhancers" as a shorthand for any potential regulatory regions in the genome) method can integrate various types of functional information, including chromatin accessibility, histone markers, and 3D chromatin conformation. There can be a significant distance between a gene and its regulatory regions; simply expanding the size of the window to include kilobases of genomic data around each gene will include too many non-causal SNPs, giving rise to power loss, as well as difficulties in results interpretation[9]. Our proposed framework can enhance statistical power for identifying new regions of association in the noncoding genome. We particularly focus on integration of 3D spatial information, which has not yet been fully exploited in most WGS association testing studies. Our method allows users to input broadly

defined regulatory/enhancer regions and then select those which are most likely relevant to a given phenotype, in a statistically powerful framework.

Given our incomplete understanding of chromatin conformation and enhancer annotation, an annotation agnostic approach such as SCANG does have some advantages, in that no prior information is needed for rare variant testing. However, our simulations and the real data example presented here demonstrate the advantages of our eSCAN method, which can flexibly accommodate multiple types of annotation information and shows significant power gains over SCANG, as well as a lower false positive rate in different scenarios for both continuous and dichotomous traits. These advantages are demonstrated in our application of eSCAN to TOPMed WGS analyses of four blood cell traits in the Women's Health Initiative (WHI) study, with replication in Jackson Heart Study (JHS).

The eSCAN procedure can be split into two steps: a *p*-value computing step and a decision-making step (using a *p*-value threshold). First, for each enhancer, set-based *p*-values are calculated by fastSKAT, which applies randomized singular value decomposition (SVD) to rapidly analyze much larger regions than standard SKAT, and then p-values are "averaged" by the Cauchy method via ACAT [4]. Second, eSCAN calculates two types of significance threshold. The first is an empirical data-driven threshold computed by Monte Carlo simulation on the basis of a common distribution of *p*-values; the second is an analytical estimation by extreme value distribution[10]. eSCAN then defines the enhancers with *p*-values below the threshold as significant. Further details are in the **Supplemental Methods**.

We next evaluated the performance of eSCAN using simulated data under the null model (more details in **Supplemental Methods**). On average, each simulated enhancer had a length of 4025 bp and contained 122 variants with MAF below 5%. For both continuous and dichotomous simulations, we applied eSCAN to 1,000 replicates with sample sizes of 2,500,

5,000 and 10,000, respectively, and set the genome-wide type I error rate at 0.05. Under all scenarios, our method has a well-controlled genome-wide type I error rate (**Table 1**).

To assess eSCAN under the alternative model, we applied eSCAN and two SCANGs, i.e. the default SCANG and enhancer based SCANG, to a wide range of simulated scenario to benchmark their performances in terms of power and false positive rate, using four metrics, namely causal-variant detection rate, causal-enhancer detection rate, variant false positive rate and enhancer false positive rate (more details in **Supplemental Methods**). For continuous traits, both the enhancer-based SCANG and our eSCAN analysis showed higher power than the default SCANG, at both the variant level and the enhancer level (**Fig. 2a-b**), for all tested sample sizes, suggesting the benefit of aggregating variants using enhancer information. Notably, the power gain between eSCAN and enhancer-based SCANG is much more pronounced than that between enhancer-based SCANG and default SCANG. eSCAN increases the variant-level power by 23.50%, 45.94% and 27.98% for the three tested sample sizes, respectively; and boosts the enhancer-level power by 17.60%, 45.47% and 24.14%, respectively. With respect to false positive rate, eSCAN showed a remarkably lower false positive rate than those from the two SCANG procedures, at both the variant-level and enhancer-level (**Fig. 2c-d**).

These results demonstrate eSCAN's capabilities to powerfully and accurately detect causal enhancers. We further evaluated eSCAN in more simulation scenarios to verify eSCAN's robustness to dichotomous traits and the proportion of causal enhancers, as well as the proportion of causal variants within the causal enhancers. Results show that these gains are robust to choice of parameters (**Fig. S1-3**).

To assess the performance of eSCAN in real data, we compared eSCAN to both enhancer based SCANG and the default SCANG using WGS data in 10,727 discovery samples from the Women's Health Initiative (WHI) and 1,970 replication samples from the

Jackson Heart Study (JHS) (**Supplemental Methods** and **Table S1**). We only considered variants with a minor allele frequency < 5% in each cohort. Windows with a total minor allele count (MAC) < 10 were excluded from the analysis. To achieve a fair comparison, we first applied eSCAN and enhancer-based SCANG for association analysis between putative enhancers and four blood cell traits measured at baseline in WHI, white blood cell count (WBC), hemoglobin (HGB), hematocrit (HCT) and platelets (PLT), with a genome-wide error rate at the level of 0.05 by Bonferroni correction in both methods. For eSCAN, enhancers were defined using promoter capture-Hi-C (PC-HiC) data in any tested white blood cell type (including neutrophils, monocytes, and lymphocytes) for WBC, erythroblasts for HGB and HCT and megakaryocytes for PLT[11], defining any noncoding region with statistically significant interactions with a gene promoter as an enhancer region. For enhancer-based SCANG, we analysed the subset of rare variants falling into any enhancer region as defined using PC-HiC annotation (more details in **Supplemental Methods**). For the default SCANG, due to the limited computational feasibility, we only performed the analysis for WBC.

Overall, eSCAN detected 19 significant regions associated with blood cell traits while enhancer-based SCANG only detected 7 regions (**Table 2** , **Table S3** and **Fig. S4A-D**). Also, eSCAN showed consistently smaller p-values for top regions compared with enhancer-based SCANG (**Fig. S4A-D** and **Table 2**). Among the 19 genome-wide significant regions detected by eSCAN in the unconditional analysis, 4 were located within +/- 500kb of known GWAS loci and were still significant at the Bonferroni correction level of 0.05/4 after conditioning on known blood cell trait GWAS loci[12-20] (**Table 2** and **Table S2**). Also, of the significant regions, two were replicated at 0.05 level in replication samples. Note that the low replication rate is likely due in large part to the much smaller sample size of the JHS replication cohorts;

we also note as a limitation that we did not correct for multiple testing in these replication analyses, due to this small sample size. .

To more comprehensively compare the top regions of eSCAN and two SCANG procedures, enhancer-based SCANG and the default SCANG, we relaxed the significance level for WBC by using the empirical threshold (more details in **Supplemental Methods**). The detected regions by eSCAN are of shorter length and contains fewer variants and than those identified by the two SCANG variants (**Fig. S5b**). Also, each region identified by eSCAN contains a single regulatory element based on annotation from promoter capture Hi-C. By contrast, regions identified by SCANG can cross multiple regulatory regions (**Fig. S5c**), which indicates that, with the help of enhancer information, eSCAN can more effectively narrow down variants and/or regulatory regions associated with a trait of interest than SCANG. We further investigated a segment on chromosome 10 where two signals were detected by enhancer-based SCANG and four by eSCAN. The two regions from SCANG overlapped the four eSCAN signals. All four were smaller in size than the SCANG detected regions. We also note that each SCANG signal contains two eSCAN signals (**Fig. 3a-c**). We then removed the associated variants in the overlapped regions between eSCAN and SCANG (which are regions detected by eSCAN since in both cases, the eSCAN regions are subsets of the SCANG regions), and re-did SCANG analysis using the retained variants only. Both regions then became insignificant (p-values> 0.02) using SCANG (**Fig. 3d**), suggesting that the sub-regions detected by eSCAN were most likely the functional regions contributing to the original significant signal.

The computational complexity of eSCAN depends on the sample size, the number of considered enhancers along a certain chromosome, and the number of rare variants residing in enhancer regions. For JHS (n=1,970) and WHI (n=10,727) eSCAN takes an average of 3h and 26h, respectively, to examine all the sets of rare variants along one chromosome, using

our cluster computing platform with one computing node and 8Gb of memory (**Fig. S6**) while SCANG limited to enhancer regions takes an average of 2.6 days and 5.3 days respectively as more eigen-decomposition steps are performed.

We propose here eSCAN, a novel aggregation method for whole genome sequencing analysis, which can integrate various types of functional information to aggregate enhancers or putative regulatory regions from WGS data and test for association with phenotypes of interest. Our method has several important advantages: (1) it has higher power and lower false positive rate, enabling it to accurately detect more significant signals than other methods (**Fig. 2** and **S1-4**); (2) the signals identified by eSCAN are of shorter sizes, which suggests eSCAN can more accurately locate the associated variants; (3) eSCAN boosts the biological interpretation of detected signals by incorporating functional annotation; (4) it is computationally efficient (**Fig. S6**).

eSCAN can be viewed as an extension of SCANG with respect to its use of dynamic searching windows and use of the *p*-value as its test statistic[4]. But it differs from SCANG in several key ways. SCANG restricts the size of searching windows within a pre-specified range and then tests all possible windows, "randomly" identifying some large regions across the genome regardless of their biological functions. eSCAN allows more flexible and biologically meaningful searching windows that mark putative enhancer(s) (**Fig. 1**). In addition, eSCAN builds on fastSKAT, a computationally efficient approach to approximate the null distribution of SKAT statistics [21].

Based on our simulations in a variety of scenarios, eSCAN can be flexibly applied to different phenotypes, both quantitative and qualitative, and is able to detect more significant signals than competing methods with a better control over false positive rate than other WGS based methods (**Fig. 2** and **Fig. S1-3**). Using WGS data from the JHS and WHI studies, we demonstrate an enrichment of association signals using eSCAN procedure. It can detect

reported signals which are not found by SCANG procedures, indicating that it is less likely to miss important regions. In addition, the regions detected by eSCAN are of shorter size than those of SCANG on average. By removing eSCAN signals from WGS data on chromosome 10 and re-running SCANG procedures, we verify that, at least for this segment, the signals detected by eSCAN drive the significant associations in larger regions identified by SCANG (**Fig. 3; Fig. S5**), a pattern we anticipate would be true for many associated regions.

Despite the modest sample size available for our blood cell trait analysis, interesting and biologically plausible rare and low frequency variant enhancer region signals were identified in our analyses from WHI. Of the genes regulated by replicated regions, *BACH2* (regulated by a region on chromosome 6: 90,423,754-90,425,200) is a key immune cell regulatory factor and is crucial for the maintenance of regulatory T-cell function and B-cell maturation [22]. Among other interesting genes *CCL18* (regulated by a region on chromosome 17: 35,982,416-35,983,367, which was not replicated in JHS) was reported to stimulate the bone marrow overall, which could lead to increased platelets[23]. These findings suggest that the associated enhancer regions identified by eSCAN may in fact play key regulatory relevant to the biological functions of blood cells, with eSCAN finding regions were not identified using the SCANG method. We do note, however, that these findings should be considered preliminary, given our modest sample size, and could be influenced by unadjusted for selection bias in WHI TOPMed sampling (enrichment for stroke and venous thromboembolism) and lack of adjustment for a genetic relationship matrix which could better capture cryptic relatedness and differential ancestry unadjusted for by PCs. However, these issues impact eSCAN and SCANG equally, and do not change our central methods comparison findings.

With respect to the weights in fastSKAT, we used two standard MAF-based weights: one is the Beta distribution with $a_1 = a_2 = 1$ reflecting that all the variants have equal effect

size, the other is $a_1 = 1, a_2 = 25$ upweighting rarer variants. One can also use external measures by incorporating individual level functional annotations, such as FATHMM-XF[24] and STAAR[25], as the weight for each variant. Incorporation of functional evidence has demonstrated its values in variant level association studies [26; 27]. In addition, the eSCAN framework is flexible regarding its unit aggregate tests. In our implementation, we use fastSKAT because of its small computational cost, but other aggregate tests can also be used, such as SMMAT, a recently proposed test which is an efficient variant set mixed model association test [28].

Another attractive feature of eSCAN is its significance threshold. Since candidate regions are highly likely to be correlated because of either physical overlapping or LD, making the set-based *p*-values also correlated, the classic Bonferroni correction would be too conservative. While we do use a classic Bonferroni correction in our real data example from WHI, due to the small sample size available to us for replication, this is almost certainly over-conservative. eSCAN provides two estimations of significance threshold, either empirically or analytically, using the strategies from SCANG and WGScan respectively, which have demonstrated significant enrichments of signals in Li et al.[4] and He et al.[10]. In addition, although our analyses focused on unrelated individuals, it can be readily extended to related samples by replacing the generalized linear model (GLM) with the generalized linear mixed model (GLMM) in the first step[4].

One potential limitation of eSCAN is the lack of base pair resolution in defining regions important for gene regulation, due to the sparsity of reads with most Hi-C and chromatin conformation assays (leading to resolution as broad as 40 kb when assessing interactions between genomic regions). ATAC-seq data, albeit much finer resolution, still results in open chromatin peak regions that usually contain multiple rare variants, particularly as sample size increases, hurdling inference at the resolution of single base pair or single

variant. These limitations are intrinsic to the functional annotation data employed rather than to the eSCAN methodology. We anticipate that rapid technological improvements in the functional annotation datasets will continue mitigating these issues by providing increasingly finer resolution and more comprehensive data, which would render eSCAN even more valuable in the near future.

Supplemental Data Description

Supplemental Data include supplemental methods, six figures and three tables, which are included as an Excel file.

Acknowledgements

We thank Zilin Li for helpful input on SCANG methods and implementation. Y.L. is partially supported by R01HL129132, R01GM105785, and U544 HD079124. LMR is supported by R01HL129132 and KL2TR002490.

The Jackson Heart Study (JHS) is supported and conducted in collaboration with Jackson State University (HHSN268201800013I), Tougaloo College (HHSN268201800014I), the Mississippi State Department of Health (HHSN268201800015I/HHSN26800001) and the University of Mississippi Medical Center (HHSN268201800010I, HHSN268201800011I and HHSN268201800012I) contracts from the National Heart, Lung, and Blood Institute (NHLBI) and the National Institute for Minority Health and Health Disparities (NIMHD). The authors also wish to thank the staff and participants of the JHS.

The WHI program is funded by the National Heart, Lung, and Blood Institute, National Institutes of Health, U.S. Department of Health and Human Services through contracts HHSN268201600018C, HHSN268201600001C, HHSN268201600002C, HHSN268201600003C, and HHSN268201600004C. The authors thank the WHI investigators and staff for their dedication, and the study participants for making the program possible. A listing of WHI investigators can be found at: https://www-whi-org.s3.us-west-2.amazonaws.com/wp-content/uploads/WHI-Investigator-Short-List.pdf.

The views expressed in this manuscript are those of the authors and do not necessarily represent the views of the National Heart, Lung, and Blood Institute; the National Institutes of Health; or the U.S. Department of Health and Human Services.

Molecular data for the Trans-Omics in Precision Medicine (TOPMed) program was supported by the National Heart, Lung and Blood Institute (NHLBI). Genome sequencing for "NHLBI TOPMed: The Jackson Heart Study" (phs000964.v1.p1) was performed at the Northwest Genomics Center (HHSN268201100037C). Genome sequencing for "NHLBI TOPMed: Women's Health Initiative (WHI)" (phs001237) was performed by Broad Genomics (HHSN268201500014C). Core support including centralized genomic read mapping and genotype calling, along with variant quality metrics and filtering were provided by the TOPMed Informatics Research Center (3R01HL-117626-02S1; contract HHSN268201800002I). Core support including phenotype harmonization, data management, sample-identity QC, and general program coordination were provided by the TOPMed Data Coordinating Center (R01HL-120393; U01HL-120393; contract HHSN268201800001I). We gratefully acknowledge the studies and participants who provided biological samples and data for TOPMed. A list of TOPMed investigators represented by the TOPMed banner can be found at https://www.nhlbiwgs.org/topmed-banner-authorship.

Declaration of Interests

The authors have no conflicts of interest to declare.

Data and Code Availability

This paper did not generate any datasets. TOPMed data from the Women's Health Initiative is available to approved researchers through dbGaP (phs001237), with phenotype data available at phs000200. TOPMed data from the Jackson Heart Study Data is also available to

approved researchers through dbGaP (phs000964), with phenotype data available at phs000286. Data is also available with an approved manuscript proposal through https://www.jacksonheartstudy.org/ (JHS) and https://www.whi.org/ (WHI).

Web Resources

We developed an R package for the eSCAN procedure. The package is available at https://github.com/yingxi-kaylee/eSCAN.

REFERENCES

1. Morrison, A.C., Huang, Z., Yu, B., Metcalf, G., Liu, X., Ballantyne, C., Coresh, J., Yu, F., Muzny, D., Feofanova, E., et al. (2017). Practical Approaches for Whole-Genome Sequence Analysis of Heart- and Blood-Related Traits. Am J Hum Genet 100, 205-215.
2. Morrison, A.C., Voorman, A., Johnson, A.D., Liu, X., Yu, J., Li, A., Muzny, D., Yu, F., Rice, K., Zhu, C., et al. (2013). Whole-genome sequence-based analysis of high-density lipoprotein cholesterol. Nat Genet 45, 899-901.
3. Natarajan, P., Peloso, G.M., Zekavat, S.M., Montasser, M., Ganna, A., Chaffin, M., Khera, A.V., Zhou, W., Bloom, J.M., Engreitz, J.M., et al. (2018). Deep-coverage whole genome sequences and blood lipids among 16,324 individuals. Nature communications 9, 3391.
4. Li, Z., Li, X., Liu, Y., Shen, J., Chen, H., Zhou, H., Morrison, A.C., Boerwinkle, E., and Lin, X. (2019). Dynamic Scan Procedure for Detecting Rare-Variant Association Regions in Whole-Genome Sequencing Studies. Am J Hum Genet 104, 802-814.
5. Wu, M., Lee, S., Cai, T., Li, Y., Boehnke, M., and Lin, X. (2011). Rare-variant association testing for sequencing data with the sequence kernel association test. American journal of human genetics 89, 82-93.
6. Farh, K.K., Marson, A., Zhu, J., Kleinewietfeld, M., Housley, W.J., Beik, S., Shoresh, N., Whitton, H., Ryan, R.J., Shishkin, A.A., et al. (2015). Genetic and epigenetic fine mapping of causal autoimmune disease variants. Nature 518, 337-343.
7. Onengut-Gumuscu, S., Chen, W.-M., Burren, O., Cooper, N.J., Quinlan, A.R., Mychaleckyj, J.C., Farber, E., Bonnie, J.K., Szpak, M., Schofield, E., et al. (2015). Fine mapping of type 1 diabetes susceptibility loci and evidence for colocalization of causal variants with lymphoid gene enhancers. Nature Genetics 47, 381-386.
8. Gallagher, M.D., and Chen-Plotkin, A.S. (2018). The Post-GWAS Era: From Association to Function. Am J Hum Genet 102, 717-730.
9. Wu, C., and Pan, W. (2018). Integration of Enhancer-Promoter Interactions with GWAS Summary Results Identifies Novel Schizophrenia-Associated Genes and Pathways. Genetics 209, 699.

10. He, Z., Xu, B., Buxbaum, J., and Ionita-Laza, I. (2019). A genome-wide scan statistic framework for whole-genome sequence data analysis. Nature communications 10, 3018.
11. Javierre, B.M., Burren, O.S., Wilder, S.P., Kreuzhuber, R., Hill, S.M., Sewitz, S., Cairns, J., Wingett, S.W., Várnai, C., Thiecke, M.J., et al. (2016). Lineage-Specific Genome Architecture Links Enhancers and Non-coding Disease Variants to Target Gene Promoters. Cell 167, 1369-1384.e1319.
12. Astle, W.J., Elding, H., Jiang, T., Allen, D., Ruklisa, D., Mann, A.L., Mead, D., Bouman, H., Riveros-Mckay, F., Kostadima, M.A., et al. (2016). The Allelic Landscape of Human Blood Cell Trait Variation and Links to Common Complex Disease. Cell 167, 1415-1429.e1419.
13. Gieger, C., Radhakrishnan, A., Cvejic, A., Tang, W., Porcu, E., Pistis, G., Serbanovic-Canic, J., Elling, U., Goodall, A.H., Labrune, Y., et al. (2011). New gene functions in megakaryopoiesis and platelet formation. Nature 480, 201-208.
14. Kanai, M., Akiyama, M., Takahashi, A., Matoba, N., Momozawa, Y., Ikeda, M., Iwata, N., Ikegawa, S., Hirata, M., Matsuda, K., et al. (2018). Genetic analysis of quantitative traits in the Japanese population links cell types to complex human diseases. Nat Genet 50, 390-400.
15. Kanai, M., Akiyama, M., Takahashi, A., Matoba, N., Momozawa, Y., Ikeda, M., Iwata, N., Ikegawa, S., Hirata, M., Matsuda, K., et al. (2018). Genetic analysis of quantitative traits in the Japanese population links cell types to complex human diseases. Nat Genet 50, 390-400.
16. Pankratz, S., Bittner, S., Kehrel, B.E., Langer, H.F., Kleinschnitz, C., Meuth, S.G., and Gobel, K. (2016). The Inflammatory Role of Platelets: Translational Insights from Experimental Studies of Autoimmune Disorders. Int J Mol Sci 17.
17. van der Harst, P., Zhang, W., Mateo Leach, I., Rendon, A., Verweij, N., Sehmi, J., Paul, D.S., Elling, U., Allayee, H., Li, X., et al. (2012). Seventy-five genetic loci influencing the human red blood cell. Nature 492, 369-375.
18. Chen, M.H., Raffield, L.M., Mousas, A., Sakaue, S., Huffman, J.E., Moscati, A., Trivedi, B., Jiang, T., Akbari, P., Vuckovic, D., et al. (2020). Trans-ethnic and Ancestry-Specific Blood-Cell Genetics in 746,667 Individuals from 5 Global Populations. Cell 182, 1198-1213.e1114.
19. Vuckovic, D., Bao, E.L., Akbari, P., Lareau, C.A., Mousas, A., Jiang, T., Chen, M.H., Raffield, L.M., Tardaguila, M., Huffman, J.E., et al. (2020). The Polygenic and Monogenic Basis of Blood Traits and Diseases. Cell 182, 1214-1231.e1211.
20. Mousas, A., Ntritsos, G., Chen, M.-H., Song, C., Huffman, J., Tzoulaki, I., Elliott, P., Psaty, B., Auer, P., Johnson, A., et al. (2017). Rare coding variants pinpoint genes that control human hematological traits. PLoS genetics 13, e1006925.
21. Lumley, T., Brody, J., Peloso, G., Morrison, A., and Rice, K. (2018). FastSKAT: Sequence kernel association tests for very large sets of markers. Genetic epidemiology 42, 516-527.
22. Afzali, B., Grönholm, J., Vandrovcova, J., O'Brien, C., Sun, H.W., Vanderleyden, I., Davis, F.P., Khoder, A., Zhang, Y., Hegazy, A.N., et al. (2017). BACH2 immunodeficiency illustrates an association between super-enhancers and haploinsufficiency. Nature immunology 18, 813-823.
23. Wimmer, A., Khaldoyanidi, S.K., Judex, M., Serobyan, N., DiScipio, R.G., and Schraufstatter, I.U. (2006). CCL18/PARC stimulates hematopoiesis in long-term bone marrow cultures indirectly through its effect on monocytes. Blood 108, 3722-3729.

24. Rogers, M.F., Shihab, H.A., Mort, M., Cooper, D.N., Gaunt, T.R., and Campbell, C. (2018). FATHMM-XF: accurate prediction of pathogenic point mutations via extended features. Bioinformatics 34, 511-513.
25. Li, X., Li, Z., Zhou, H., Gaynor, S.M., Liu, Y., Chen, H., Sun, R., Dey, R., Arnett, D.K., Aslibekyan, S., et al. (2020). Dynamic incorporation of multiple in silico functional annotations empowers rare variant association analysis of large whole-genome sequencing studies at scale. Nature Genetics 52, 969-983.
26. Pickrell, J.K. (2014). Joint analysis of functional genomic data and genome-wide association studies of 18 human traits. Am J Hum Genet 94, 559-573.
27. Yang, J., Fritsche, L.G., Zhou, X., and Abecasis, G. (2017). A Scalable Bayesian Method for Integrating Functional Information in Genome-wide Association Studies. Am J Hum Genet 101, 404-416.
28. Chen, H., Huffman, J.E., Brody, J.A., Wang, C., Lee, S., Li, Z., Gogarten, S.M., Sofer, T., Bielak, L.F., Bis, J.C., et al. (2019). Efficient Variant Set Mixed Model Association Tests for Continuous and Binary Traits in Large-Scale Whole-Genome Sequencing Studies. Am J Hum Genet 104, 260-274.

Figure titles and legends

Figure 1: An illustration of eSCAN.

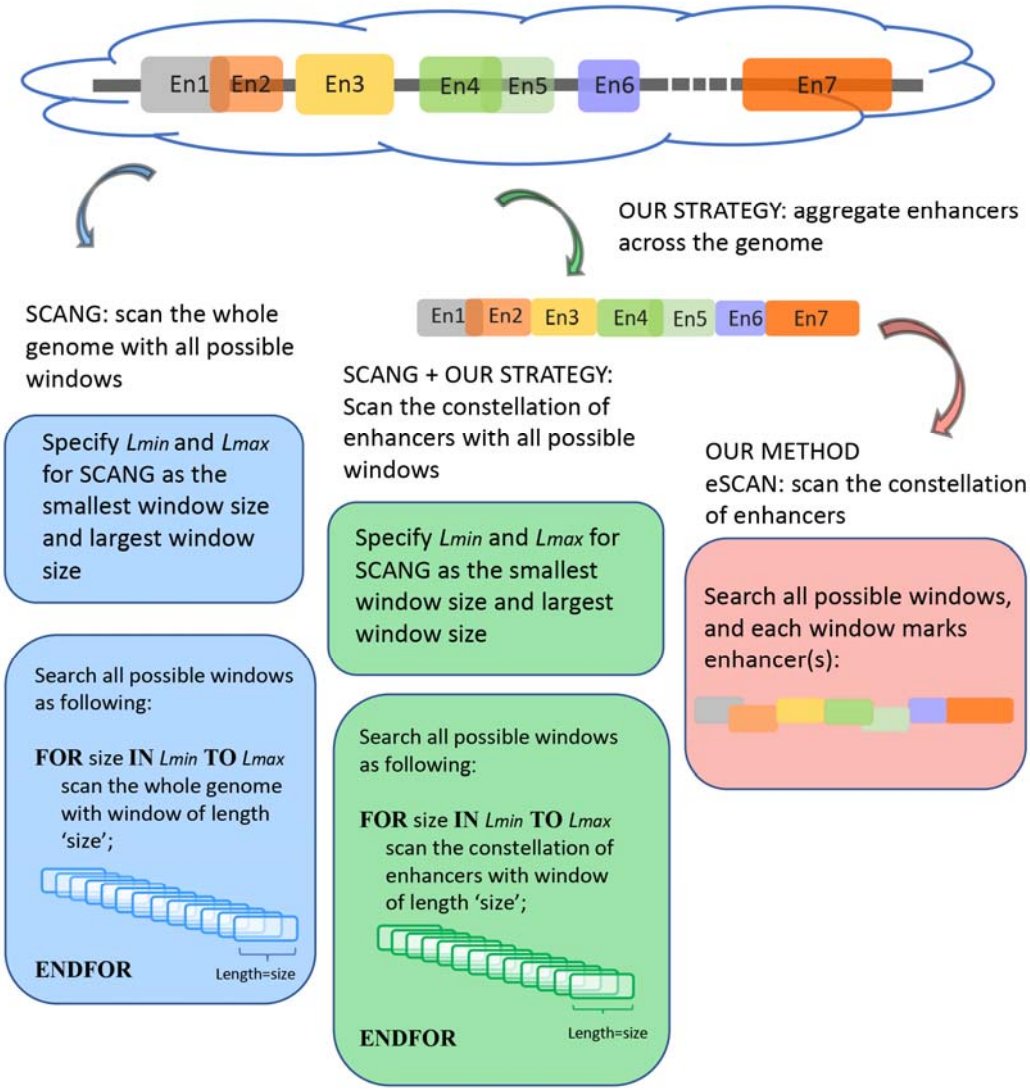
En1
En2
En3
En4
En5
En6
En7
OUR STRATEGY: aggregate enhancers across the genome
SCANG: scan the whole genome with all possible windows
Specify Lmin and Lmax for SCANG as the smallest window size and largest window size
Search all possible windows as following:
FOR size IN Lmin TO Lmax
scan the whole genome with window of length 'size';
ENDFOR
Length=size
SCANG + OUR STRATEGY: Scan the constellation of enhancers with all possible windows
Specify Lmin and Lmax for SCANG as the smallest window size and largest window size
Search all possible windows as following:
FOR size IN Lmin TO Lmax
scan the constellation of enhancers with window of length 'size';
ENDFOR
Length=size
OUR METHOD
eSCAN: scan the constellation of enhancers
Search all possible windows, and each window marks enhancer(s):

Figure 2: Power and false positive Rate Comparison of eSCAN and SCANG for Continuous Traits as Sample Size Changes.

We evaluated the performance of eSCAN for continuous traits analysis as sample size changes. The total sample sizes considered were 2,500, 5,000 and 10,000. For each configuration, we compared three methods: eSCAN and two SCANGs: enhancer-based SCANG (aggregating enhancers across the genome) and default SCANG (scan the whole genome). We evaluated power and false-positive performance at both variant-level and enhancer-level.

Panel **a** presents power at the variant-level (a.k.a. causal-variant detection rate). Panel **b** presents power at enhancer-level(a.k.a. causal-enhancer detection rate). Panel **c** presents results of the false positive rate at variant-level. Panel **d** presents the false positive rate at the enhancer-level.

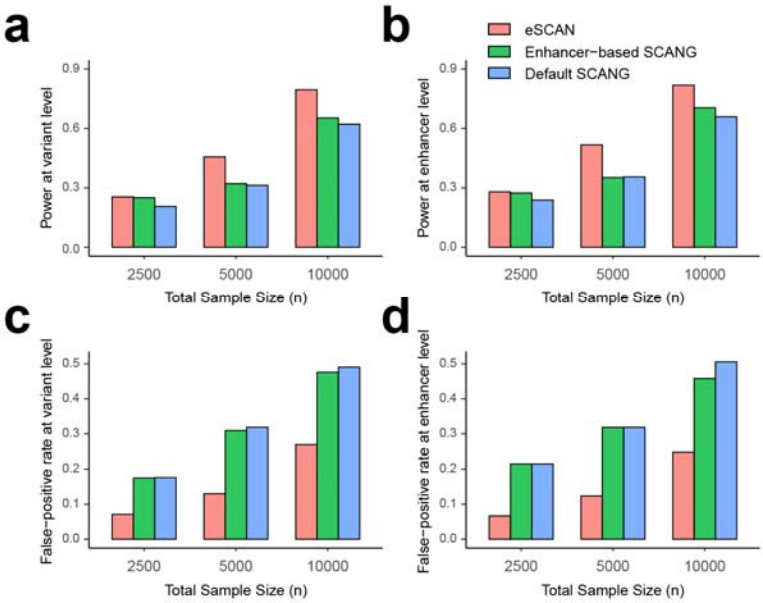

Figure 3: A segment on chromosome 10 where two signals were detected by SCANG and four by eSCAN.

We further investigated a segment on chromosome 10 where two signals were detected by SCANG and four by eSCAN. The two regions from SCANG (chr10: 113,767,467-113,773,998 with p-value=2.66×10^(-7) and chr10: 113,774,365-113,779,787 with p-value=7.81×10^(-7)) overlapped the four eSCAN signals (**a**). All four is smaller in size than the SCANG detected regions (**b**). Specifically, eSCAN detected chr10: 113,770,735-113,773,147 with p-value=2.84×10^(-6); chr10: 113,773,148-113,774,046 with p-value=6.59×10^(-6); chr10: 113,774,047-113,775,910 with p-value=9.55×10^(-6) and chr10: 113,775,911-113,778,291 with p-value=1.92×10^(-5)). Each SCANG signal contains two eSCAN signals (**c**). We then removed the associated variants in the overlapped regions between eSCAN and SCANG (which are regions detected by eSCAN since in both cases, the eSCAN regions are subsets of the SCANG regions), and re-did SCANG analysis using the retained variants only. Both regions then became insignificant (p-values>0.02) using SCANG (**d**), suggesting that the sub-regions detected by eSCAN were most likely the functional regions contributing to the original significant signal.

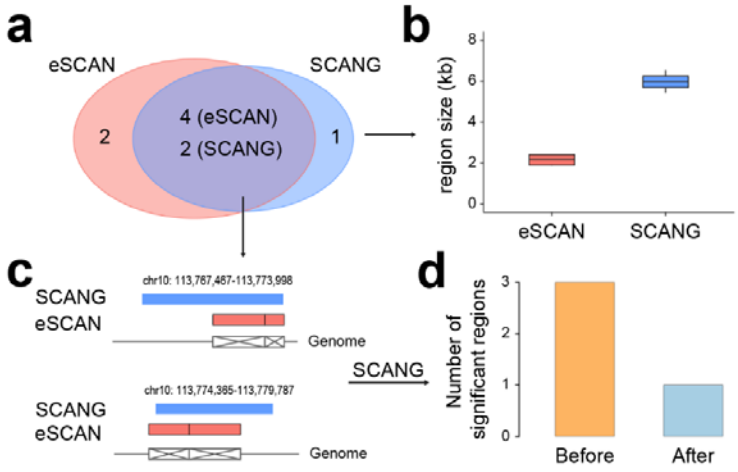

Tables

Table 1: Genome-wide empirical type 1 error rates of eSCAN from simulation studies, shown for different sample sizes and trait distributions.

Sample size	**n=2,500**	**n=5,000**	**n=10,000**
Continuous Traits	0.003	0.002	0.001
Dichotomous Traits	0.001	0.001	0.002

Table 2: Significant results by eSCAN for blood cell traits in TOPMed whole genome sequencing data. Chromosome, start position (hg38), end position (hg38), p-value in discovery samples (Women's Health Initiative, WHI), p-value of nearest region tested by enhancer-based SCANG, known GWAS loci within +/- 500kb, associated trait (HGB, hemoglobin, PLT, platelet count, WBC, white blood cell count), p-value in the replication samples (Jackson Heart Study, JHS), gene(s) regulated by the detected region, total minor allele count (MAC) in the discovery samples, total MAC in the replication samples.

Chr	Start	End	P-value	P-value by enSCANG (strat:end)	Known GWAS	Trait	P-value (replication)	Regulated gene	MAC	MAC (replication)
5	178,360,084	178,360,305	9.54E-10	5.82E-02 (178,342,330: 178,367,547)	No	HGB	0.56	*COL23A1*	22	30
8	98,026,570	98,027,915	1.01E-08	9.24E-04 (98,023,407: 98,078,162)	No	HGB	0.11	*MTDH; LAPTM4B; RNU7-177P; Y_RNA; MATN2; RPS23P1*	11	11
9	32,397,109	32,404,847	2.52E-08	7.75E-03 (32,289,232: 32,422,553)	Yes	HGB	0.42	*CAAP1; IFT74; RP11-337A23.3; IFNK; AL353671.1; AL353671.2; DDX58; TOPORS-AS1; TOPORS; NDUFB6; APTX; DNAJA1*	15	18
16	14,509,775	14,511,544	1.67E-08	1.78E-03 (14,479,136: 14,781,283)	No	HGB	0.76	*ERCC4; RPS26P52; MIR193B; MIR365A*	34	6
16	53,504,703	53,505,714	6.45E-07	1.04E-02 (53,483,984: 53,535,907)	No	HGB	0.80	*CHD9; RP11-467J12.4; RBL2; AKTIP; CRNDE; IRX5; LPCAT2; MMP2; CNOT1*	25	107
17	37,034,219	37,034,447	1.46E-08	7.13E-04 (37,016,046: 37,060,384)	No	HGB	0.63	*DHRS11; DHRS11; MRM1*	13	4
1	103,517,128	103,522,214	2.55E-14	1.26E-02 (103,476,276: 103,518,492)	No	PLT	0.51	*ACADM; RP4-682C21.5; RP11-57H12.3; RWDD3; SASS6; COL11A1*	25	27
1	37,597,769	37,598,312	4.92E-27	5.37E-03 (37,588,746: 37,598,034)	No	PLT	0.46	*RP1-43E13.2; UBR4; LINC01137; ZC3H12A; MEAF6; C1orf109; CDCA8; C1orf122; YRDC; MTF1; RP11-109P14.10; FHL3; UTP11L*	25	13
1	39,128,051	39,129,395	6.32E-12	2.42E-02 (39,127,407: 39,129,821)	No	PLT	NA	*RP11-420K8.1; KIAA0754; BMP8A; PABPC4*	28	NA

6	148,155,161	148,157,516	1.29E-09	3.20E-02 (148,142,817: 148,156,466)	No	PLT	0.70	*SAMD5*	40	18
6	90,423,754	90,425,200	3.46E-09	4.86E-02 (90,422,386: 90,424,684)	No	PLT	0.01	*MDN1; snoU13; GJA10; Y_RNA; RP11-63K6.7; RP3-512E2.2; BACH2*	15	5
9	113,408,320	113,408,738	6.24E-11	4.72E-04 (113,286,449: 113,425,110)	No	PLT	0.10	*CDC26; PRPF4; RP11-168K11.2*	36	17
12	27,242,306	27,243,091	2.34E-10	1.16E-02 (27,239,926: 27,242,793)	No	PLT	0.02	*CASC1; LYRM5; ASUN; FGFR1OP2; RP11-421F16.3; TM7SF3; MED21; CCDC91; RP11-967K21.1; C12orf29; C12orf50*	40	12
15	75,460,830	75,464,641	1.60E-07	7.61E-03 (75,455,032: 75,466,056)	No	PLT	0.29	*CTD-2026K11.3; SNUPN; CTD-2026K11.1; IMP3;SNX33*	38	14
17	35,982,416	35,983,367	3.24E-15	2.14E-03 (35,974,330: 36,042,136)	Yes	PLT	0.12	*CCL18; AC069363.1; ZNHIT3*	14	31
1	35,978,873	35,979,878	1.17E-19	9.08E-03 (35,918,715: 36,037,384)	Yes	WBC	0.11	*AGO1*	17	11
1	166,941,439	166,942,948	2.81E-09	2.68E-03 (166,881,863: 167,002,809)	Yes	WBC	0.34	*RP11-102C16.3*	10	5
10	51,376,256	51,378,263	6.10E-08	1.65E-02 (51,281,521: 51,397,833)	No	WBC	0.73	*RP11-96B5.3*	21	74
14	96,608,711	96,610,505	3.67E-11	5.06E-03 (96,599,488: 96,619,536)	No	WBC	0.25	*CTD-2200A16.1; U6*	15	12